PROCEEDINGS OF SCIENCE

High fluence effects on silicon detectors: An overview of the state of the art of radiation resistant detector characterisation by the CERN RD50 collaboration.

S. Wonsak* **on behalf of the RD50 collaboration**
University of Liverpool
E-mail: sven.wonsak@cern.ch

The CERN RD50 collaboration has the aim to investigate radiation hard semiconductor devices for very high luminosity colliders. This is done by looking into four key aspects: Defect/material characterization, detector characterization, new structures and full detector systems.
After the Phase II upgrade of the Large Hadron Collider (LHC) the luminosity will increase and therefore the radiation level for the silicon detectors. They have to be able to operate at fluences of up to 2×10^{16} n_{eq}/cm^2. To cope with this, new semiconductor sensor technologies have been developed. This article will give a brief overview of the latest results of the RD50 collaboration for the characterization of 3D detectors, HV-CMOS pixel detectors, low gain avalanche detectors (LGAD) and sensors with slim/active edge.

The 25th International workshop on vertex detectors
September 26-30, 2016
La Biodola, Isola d'Elba, ITALY

*Speaker.

PoS(Vertex 2016)032

1. Intoduction

With the upgrade of the large hadron collider (LHC) towards high luminosity after the long shut down of 2024-2026 the integrated luminosity is expected to reach 3000 fb^{-1}. Semiconductor sensors in the two multi-purpose experiments ATLAS and CMS will be exposed to fluences equivalent to more than 1×10^{16} n_{eq}/cm^2. Beside the radiation hardness, the silicon sensors will also need a high granularity to cope with the occupancy and a low material budget. The CERN RD50 collaboration [1] has the mandate to develop and characterize radiation hard semiconductor sensors for very high luminosity colliders. 52 institutes from Europe, Asia, North-America and the Middle East participate in this common goal. 3D and HV-CMOS detectors are a promising alternative to standard pixel/strip devices, while Low Gain Avalanche Detectors improve the signal strength and can be used for example in pad diodes for timing measurements. Furthermore, the use of slim/active edge technology reduces the inactive area.

2. Measurement Systems

The Transient Current Technique (TCT) is used to investigate the electric field profile and the collected charge of silicon detectors. A red or infrared laser is used to induce electron/hole pairs either in the silicon bulk (infrared) or on the surface of the device (red). The amplified signal is read out with an oscilloscope. In a surface scan the laser points towards the top or bottom of the sensor and allows a detailed analysis of the surface. For the characterization of the electric field an infrared laser needs to point to the detector edge (eTCT, [2]). Figure 1 shows a schematic view of a TCT system with either a red or infrared laser: the infrared laser light can pass through the whole sensor thickness creating electron-hole pairs along its way. With the red laser the charge carriers are only created in the surface. In this example of a n-in-p sensor the electrons created at

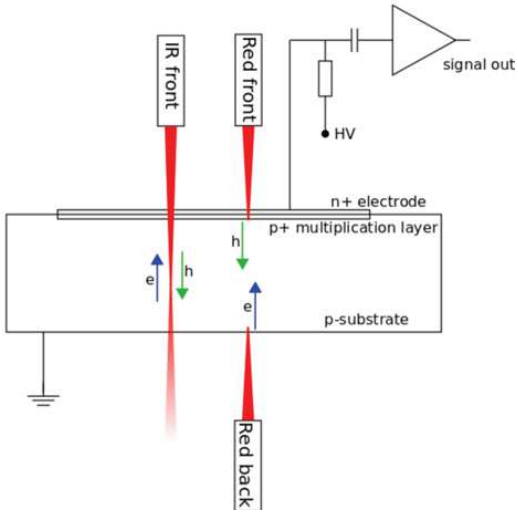

Figure 1: Schematic working principle of front/back TCT illumination of a silicon sensor and the charge carrier generation [5].

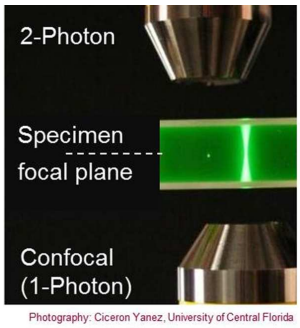

Figure 2: Comparison of charge carrier generation of standard single-photon TCT with two-photon absorption -TCT [6]. A fluorescent liquid is used to visually demonstrate the area in which the charge carriers are generated.

the front surface are immediately collected by the electrode while the holes have to travel to the backside. If the laser light is applied to the backside the holes are immediately collected by the backside implant while the electrons need to travel to the front side. Therefore red laser light is used to investigate the charge transport of electrons or holes inside a silicon sensor.

A new measurement method, based on the TCT idea, is the Two Photon Absorption (TPA-TCT, [3, 4]). In the standard TCT method a single photon has enough energy to create an electron/hole pair. For the TPA-TCT the energy of a photon is lower, but if two photons arrive at the same spatial coordinate within approximately 100 attoseconds the total energy is sufficient for the charge carrier generation. Electron/hole pairs are only generated in a very localized position which allows a high resolution 3D mapping of the device. Figure 2 shows the difference between the standard single photon TCT and the TPA-TCT: the single photons generate fluorescence light along the whole path in the liquid specimen forming the typical laser intensity profile with a minimum in the focal plane. The two-photon system creates a point-like fluorescence reaction in the focal plane, emphasizing the advantages of this method.

3. 3D Detectors

For planar sensors the readout doped region is realized at the surface of the device. The full depletion depth is equivalent to the bulk thickness. 3D detectors use a different concept: the junction and ohmic region are realized as columns in the detector bulk. The full depletion voltage is defined by the distance distance between junction and ohmic column, not by the bulk width, and for the same reason the drift distance is reduced as well. 3D sensors are used as pixel detectors where each collecting column can be read individually or few columns can be connected. The columns can be either all etched from the top or from the top and bottom [7], separating field columns and readout electrodes. Because of their complexity the production yield compared to standard pixel detectors is lower and the price for a detector higher. The higher capacitance of 3D devices results in higher noise. Additional the area at the column position is not sensitive and together with

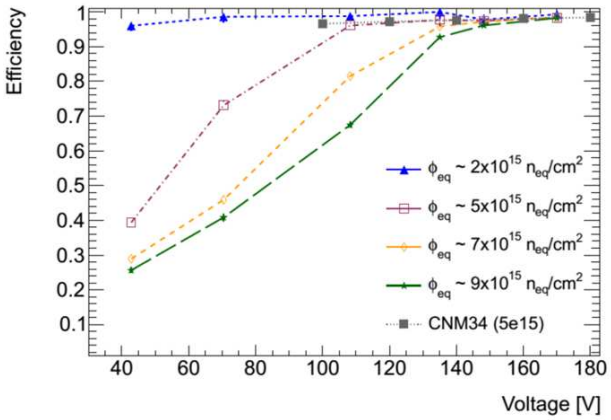

Figure 3: Efficiency of a non-uniform irradiated 3D sensor for different fluences up to 9×10^{15} n_{eq}/cm^2[10]. The 3D sample CNM34 was irradiated with 23 MeV protons at Karlsruhe to a fluence of 5×10^{15} n_{eq}/cm^2 [11].

the non-uniform electric field results in a non-uniform response. Enhanced radiation hardness is expected due to reduced trapping and a reduced depletion voltage, while the total ionised charge is determined by the substrate thickness. First 3D detectors are used in the ATLAS IBL [8] as well as the ATLAS Forward Proton detector [9].

3D detectors have undergone an extensive test program which includes irradiations and efficiency studies in test-beams. The collected charge efficiency of a sensor of the IBL/AFP generation with 67 µm inter-electrode distance, non-uniformly irradiated with 24 GeV protons at CERN and read out with a FE-I4 pixel chip, has shown that even at the highest fluence of 9.1×10^{15} n_{eq}/cm^2 the sensor has a 97.8% efficiency at 170 V (figure 3) [10]. An irradiated planar sensor with the same fluence would require a higher voltage to achieve the same efficiency.

4. Low Gain Avalanche Detectors

Low Gain Avalanche Detectors (LGAD) are silicon sensors with built-in signal amplification. The amplification is due to the high field region realized by an additional doping layer below the charge carrier collection electrode. For example in a n-in-p sensor an additional p-doping is used as multiplication layer. This creates a signal amplification with noise levels similar to standard PIN diodes [12], but the multiplication needs to be small enough not to saturate the front-end readout chip.

LGAD sensors have a characteristic signal when measuring the device with the TCT system from the backside, as can be seen in figure 4. The electrons from the laser induce a primary current in the readout electrode. When they reach the multiplication layer they create secondary electron/hole pairs. The holes then have to travel to the backside which results in an increased induced current, shown as high signal peak. For higher bias voltages the onset of the multiplication is clearly visible as knee in the current profile.

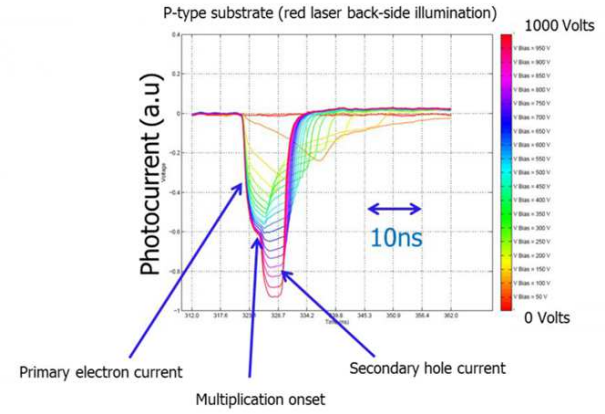

Figure 4: Backside illuminated TCT signal of a LGAD [13].

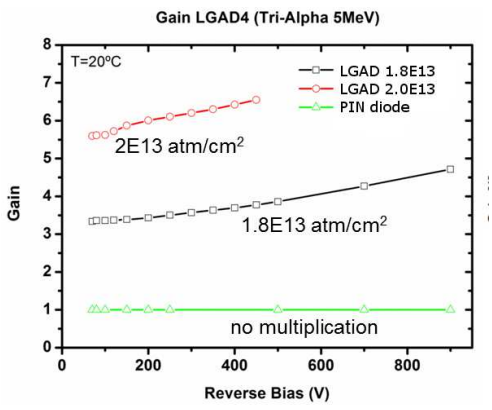

Figure 5: Gain of LGADs with different multiplication layer doses [14].

The multiplication factor of the LGAD devices is linked to the doping concentration of the multiplication layer. Devices with different doping profile values and dopant elements have been produced by CNM in Barcelona [15, 12]. It can be seen in figure 5 that for boron implant dose

an implantation dose increase from 1.8×10^{13} atoms/cm^2 to 2×10^{13} atoms/cm^2 increases the gain by nearly a factor two, which makes the control of the implantation dose of the high field region crucial to control the gain.

Measurements with 300 µm thick LGAD sensors (beam test and laser) have shown a time resolution of less then 200 ps [16], which is in good agreement with simulations using Weightfield 2 [18]. The measurements and simulations further show that a reduction of the capacitance reduces the time resolution. By also reducing the sensor width to 50 µm the simulations show that a time resolution of approximately 30 ps can be achieved with LGAD sensors of a gain of 10. A test of a 75 µm thick LGAD device with a gain of 5 has shown a time resolution of (41±7) ps [17] which further confirms the simulations.

5. HV-CMOS Detectors

A new way of producing particle detectors is the commercially available HV-CMOS technology. The main application here are pixel sensors that benefit from in-pixel amplification. It is also possible to include processing electronics in the pixel cell, creating a fully monolithic detector which does not need a front-end readout chip. The CMOS manufacturing technology allows the production of pixel with a size of $50 \times 50\,\mu m^2$ or smaller. An alternative to bump-bonding for non-monolithic detectors is capacitive coupling: by placing only the pre-amplifier inside the pixel cell it is possible to capacitive couple the sensor with the front-end chip by a thin glue layer.

Figure 6 shows a exemplary cross section of a HV-CMOS pixel detector layout. A deep n-well forms the pn-junction with the p-substrate of the bulk. Separate bias contacts to the substrate and the deep n-well allow the application of high voltage. Inside the deep n-well a p-well is used to allow N-MOS structures while P-MOS structures can be directly processed into the deep n-well. The depletion region of the sensor starts at the deep n-well and extends into the p-type substrate. Electron/hole pairs, generated in this region by a charged particle, are separated and the electrons drift towards the deep n-well, where they are collected. The p-substrate can have a resistivity from 10 Ω·cm up to 3900 Ω·cm, depending on the manufacturing foundry and the requirements.

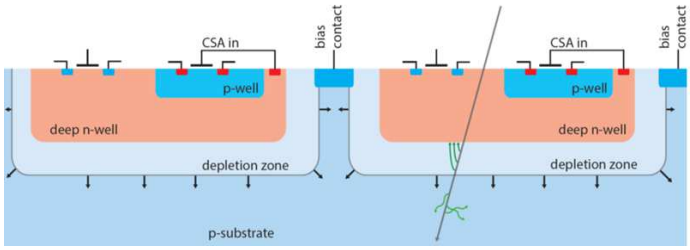

Figure 6: Examplary cross section of a HV-CMOS pixel detector layout with the different doped regions [19].

The H35Demo chip[1], produced in the AMS technology with substrate resistivities from 20 Ω·cm (the standard resistivity with HV-AMS 0.35 um) to 1000 Ω·cm, was extensively tested by different RD50 groups [20]. Figure 7 shows the layout of a single pixel cell of the H35demo device. HV

[1] An ATLAS upgrade project

connection points at each side are used for top-biasing the device. The deep n-well, realizing the pn-junction, is divided into three connected parts of which the central is used for the nMOSi and pMOSi realisation. A dedicated 3×3 pixel matrix at one edge of the device is used for TCT measurements. It does not have nMOSi or pMOSi structures and the SNTUB layers are connected to the input of the current amplifier, not to vdda. The signal from the 'central' pixel can be individually read out while the signals of the eight surrounding pixels are hardware connected (see also figure 8 right). A top TCT measurement result (infrared laser) of this test structure is shown in figure 8. The metal lines are clearly visible as regions with lower collected charge and it is possible to distinguish the three different n-wells in the graph. The 'central' well shows more collected charge than the two 'external' wells due to laser reflections over a polysilicon layer above the smaller outer n-wells. A edge-TCT measurement, shown in figure 9, shows a uniform collected charge of the whole pixel cell. The three wells can be distinguished by the dips, caused by the electric field from the n-wells.

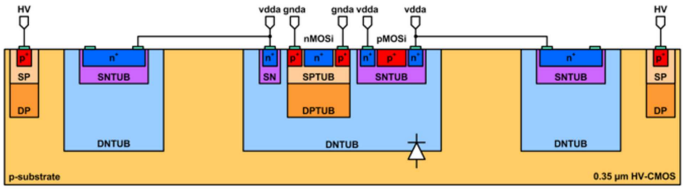

Figure 7: H35Demo HV-CMOS demo pixel sensor TCT test structure [22].

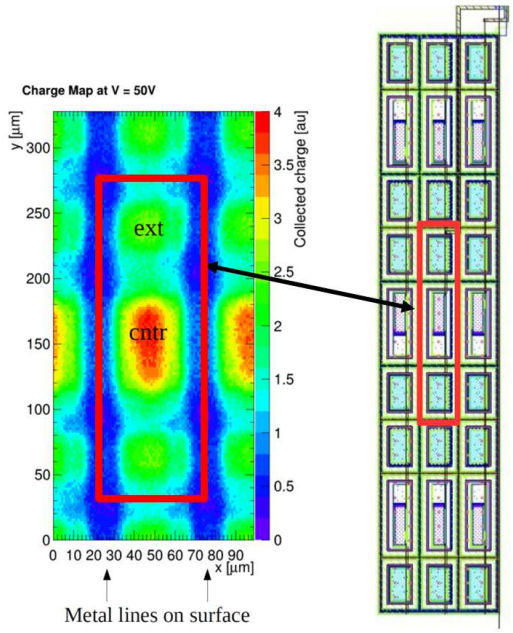

Figure 8: Collected charge measured with top TCT of a H35Demo test structure [23]. The right picture shows the 3×3 pixel test structure.

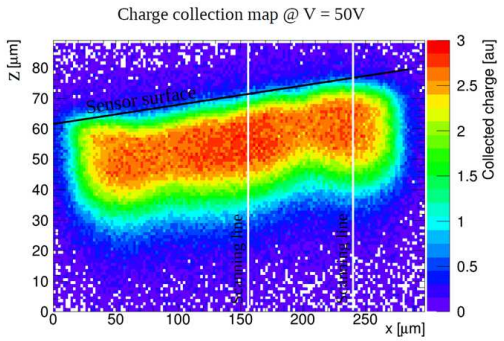

Figure 9: Collected charge measured with edge-TCT of a H35Demo test structure [23].

HV-CMOS devices of the three foundries AMS, LFoundry and XFAB have been irradiated with neutrons at the TRIGA mark 3 reactor in Ljubljana [21] to fluences up to 1×10^{16} n_{eq}/cm^2. The

main difference between the foundries is the substrate resistivity: AMS 20 Ω·cm; XFAB 100 Ω·cm; LFoundry 2000 Ω·cm [24]. Figure 10 shows the collected charge at different fluences for the XFAB devices. With increasing irradiation fluence, the charge collection width increases up to the maximum value at 5×10^{14} n_{eq}/cm^2. For higher fluences, the width decreases. The increase can be explained by the initial acceptor removal. When the acceptor removal is finished the width decreases and the space charge concentration increases with increasing fluence [25]. This behaviour has been observed for all foundries and is related to the resistivity. The reversal point changes for different samples: For 20 Ω·cm (AMS) it is at approximately 2×10^{15} n_{eq}/cm^2, while the charge collection width decrease of high resistivity LFoundry devices has been observed for irradiation fluences higher than 5×10^{13} n_{eq}/cm^2.

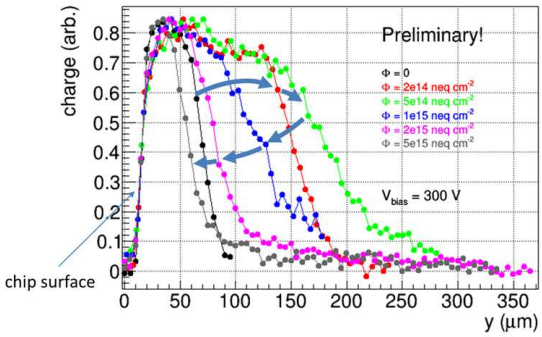

Figure 10: Charge collection width of XFAB HV-CMOS sensors, irradiated to fluences from 2×10^{14} n_{eq}/cm^2 to 5×10^{15} n_{eq}/cm^2 in comparison with an unirradiated device [24].

The two-photon-absorption TCT method has been used to characterize a HV-CMOS test structure, shown in figure 11. In the left picture the cross section of the tested device can be seen: a deep n-well within a p-substrate, without any N-MOS or P-MOS structures. Bias voltage is applied to the n-wells and the smaller p-wells inbetween them (top biasing). The charge collection map allows a clear distinction between the n-well and the surrounding substrate with a depleted layer of approximately 15 µm. Calculating the lapse of time between the beginning and the end of the signal results in the right graph. A short time lapse indicates the drift region with fast charge carrier movement while a larger time lapse points to the diffusion region. The total collection time has been limited to 20 ns for this plot.

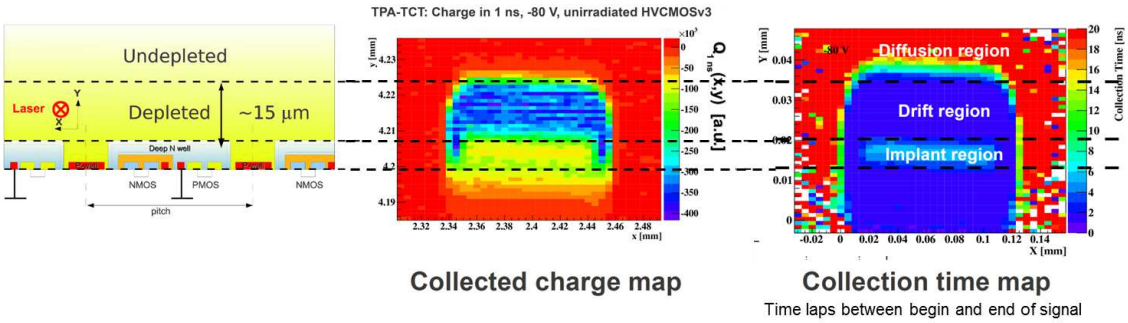

Figure 11: TPA-TCT measurement of a HV-CMOS test structure [26, 3].

6. Slim/Active Edge

Reducing the dead space at the sensor edges increases the coverage of active area in large detector systems. In pixel detectors the distance between the outermost pixel and the physical edge of the silicon device can be approximately 1 mm. This space - that is inactive for the detections of particles - is required for the termination structures (guard rings and bias ring) and in order to have a sufficient distance between active area and scribe line. Within the RD50 collaboration the possibility of reducing this area is under investigation. Scribing, Cleaving and subsequent Passivating (SCP [27]) reduces the inactive area and provides a good performance for slim edge sensors. In an alternative method trenches close to the active area are etched into the inactive area with a distance of 50-200 µm to the outermost pixel. Four-quadrant implantation can be used to dope the edges of the sensor and create active-edge devices [28]. A direct comparison of the edge efficiency for unirradiated active edge and slim edge pixel detectors with a thickness of 100 µm can be seen in figure 12. The efficiency has been measured in a test-beam and it shows that in the case of the slim edge the efficiency decreased by 50% at the inner edge of the guard ring. Whereas for the active edge device the efficiency is reduced by 50% at the outer edge of the guard ring, increasing the sensitive area. The smearing of the efficiency graphs is caused by the measurement resolution of approximately 18 µm.

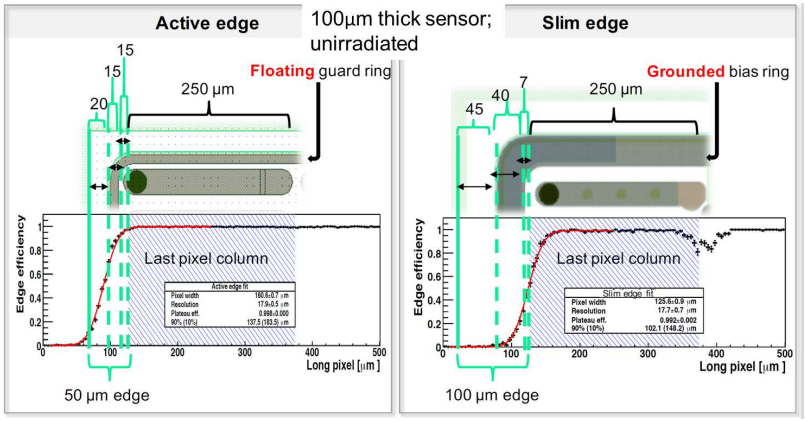

Figure 12: Performance comparison of active edge and slim edge pixel detectors [29].

7. Summary

The CERN RD50 collaboration has the mandate to develop and characterize radiation hard semiconductor sensors for very high luminosity colliders. In this article results of new detector technologies have been presented. 3D detectors decouple the depletion depth from the bulk thickness. It has been shown that a 3D device irradiated to 9.1×10^{15} n_{eq}/cm^2 shows an efficiency of 97.8% already at 170 V, whereas a conventional planar detector would require a higher bias voltage to achieve this after the same irradiation fluence.

Low Gain Avalanche Detectors utilize avalanche ionization in a dedicated doped multiplication layer to increase the signal, while having the same noise level like standard detectors. The

characteristic TCT signal with the multiplication peak has been introduced. Measurements of the gain for detectors with different multiplication layer doping concentrations have shown that an increase of approximately 11% to 2×10^{13} atoms/cm^2 results in an increase of the gain by nearly a factor 2. This shows that the choice of the doping parameters is crucial because the signal needs to be small enough not to saturate the front-end readout chip.

Measurement results of different HV-CMOS devices have been presented. Edge TCT measurements of the H35Demo device have shown a uniform charge collection profile for the three deep n-wells in a pixel cell. For AMS, XFAB and LFoundry the charge collection width depends on the irradiation fluence and the substrate resistivity. An increase because of initial acceptor removal, followed by the decrease caused by the increasing space charge concentration has been observed for all foundries with different reversal point irradiation fluences (resistivity dependent). First measurement results with the newly developed two-photon-absorption TCT (TPA-TCT) have been shown. The very good spatial resolution allows the identification of the implant as well as a discrimination between drift and diffusion region within the device.

Reducing the inactive area at the edges of sensors is beneficial for the construction of large detector systems. It has been shown that the distance between the sensor edge and the outermost pixel can be reduced to up to 50 µm for slim/active edge sensors. A comparison of the efficiency has shown that for active edge sensors the full efficiency region exceeds that of slim edge detectors.

8. Acknowledgement


This project has received funding from the European Union's Horizon 2020 research and innovation programme under grant agreement No 654168

References

[1] RD50 webpage, *http://rd50.web.cern.ch/rd50/*

[2] G. Kramberger et al., *Investigation of irradiated silicon detectors by edge-TCT*, *IEEE Trans. Nucl. Sci.* **57** (2010) 2294

[3] F.R.Palomo et al., *Two Photon Absorption and carrier generation in semiconductors*, talk at *25th RD50 workshop*, November 2014

[4] I Vila et al., *TPA-TCT: A novel Transient Current Technique based on the Two Photon Absorption (TPA) process*, talk at *25th RD50 workshop*, November 2014

[5] S. Otero Ugobono et al., *TCT measurements and analyses of proton irradiated LGADs*, talk at *28th RD50 workshop*, June 2016

[6] I. Vila et al. *Progress on the Two-Photon-Absortion TCT technique*, talk at *26th RD50 workshop*, June 2015

[7] G. Pellegrini et al., *First double-sided 3-D detectors fabricated at CNM-IMB*, http://dx.doi.org/10.1016/j.nima.2008.03.119

[8] G. Darbo, *Experience on 3D silicon sensors for ATLAS IBL*, 2015 *JINST* **10** C05001

[9] S. Grinstein et al., *Module production of the one-arm AFP 3D pixel tracker*, submitted to JINST, November 2016; *arXiv:1611.01005 [physics.ins-det]*

[10] J. Lange et al., *3D silicon pixel detectors for the High-Luminosity LHC*, 2016 *JINST* **11** C11024

[11] ATLAS IBL collaboration, *Prototype ATLAS IBL Modules using the FE-I4A Front-End Readout Chip*, 2012 *JINST* **7** P11010

[12] G. Pellegrini et al., *Technology developments and first measurements of Low Gain Avalanche Detectors (LGAD) for high energy physics applications*, http://dx.doi.org/10.1016/j.nima.2014.06.008

[13] I. Vila et al. *Signal Amplification in strip-LGAD and I-LGADs*, talk at *28th RD50 workshop*, June 2016

[14] S. Hidalgo et al. *Status of CNM developments on LGAD and iLGAD detectors*, talk at *27th RD50 workshop*, December 2015

[15] Institute of Microelectronics of Barcelona IMB-CNM webpage, *http://www.imb-cnm.csic.es/index.php/en/*

[16] H. Sadrozinski et al. *Time Resolution of UFSD*, talk at *27th RD50 workshop*, December 2015

[17] H. Sadrozinski et al. *Progress in Ultra-Fast Silicon Detectors*, talk at *28th RD50 workshop*, June 2016

[18] Weightfield 2 freeware 2D simulator for silicon and diamond detector *http://personalpages.to.infn.it/ cartigli/Weightfield2/Main.html*

[19] S. Fernandez-Perez et al. *Charge Collection Properties on a Depleted Monolithic Active Pixel Sensor using a HV-SOI process*, talk at *TWEPP 2015 - Topical Workshop on Electronics for Particle Physics*

[20] E. Cavallaro et al., *Studies of irradiated AMS H35 CMOS detectors for the ATLAS tracker upgrade*, https://arxiv.org/abs/1611.04970

[21] L. Snoj, G. Žerovnik and A. Trkov, *Computational analysis of irradiation facilities at the JSI TRIGA reactor*, *Appl. Radiat. Isot.* 70 (2012) 483

[22] E. Vilella-Figueras et al. *Prototyping of an HV-CMOS demonstrator for the High Luminosity-LHC upgrade* 2016 *JINST* **11** C01012

[23] E. Cavallaro et al. *TCT studies on AMS H35 CMOS devices for application in the ATLAS tracker upgrade*, talk at *28th RD50 workshop*, June 2016

[24] I. Mandić et al., *E-TCT measurements of irradiated HV-CMOS test structures*, talk at *28th RD50 workshop*, June 2016

[25] G. Kramberger et al. *Charge collection studies in irradiated HV-CMOS particle detectors*, 2016 *JINST* **11** P04007

[26] M. Fernandez-Garcia et al. *3D imaging of an HVCMOS using Two Photon Absorption-TCT*, talk at *28th RD50 workshop*, June 2016

[27] V. Fadeyev et al. *Update on scribe-cleave-passivate (SCP) slim edge technology for silicon sensors: Automated processing and radiation resistance*, in proceedings of *9th International 'Hiroshima' Symposium on the Development and Application of Semiconductor Tracking Detectors (HSTD-9)*, http://dx.doi.org/10.1016/j.nima.2014.05.032

[28] S. Terzo et al. *Irradiated n-in-p planar pixel sensors of different thicknesses and active edge designs*, talk at *23rd RD50 workshop*, November 2013

[29] N. Savic et al. *Performance of thin n-in-p planar pixel modules with and without active edge*, talk at *28th RD50 workshop*, June 2016